

3-Fluoropiperidines and *N*-Methyl-3-fluoropiperidinium Salts: The Persistence of Axial Fluorine

Aiming Sun,^[a] David C. Lankin,^{*[b]} Kenneth Hardcastle,^[a] and James P. Snyder^{*[a]}

Abstract: It has previously been shown that the fluorine atom in *N*-protonated 3-fluoropiperidine salts in water strongly prefers the axial orientation in the six-membered ring chairs. In the present work we examine the proposition that the *N*-methyl salts are equally disposed to present axial fluorine. Initially, we explored this point by comparing the structures of the corresponding NH_2^+ , NHMe^+ , and NMe_2^+ salts by means of density functional theory (DFT), *ab initio*, and MMFF force field calculations with and without aqueous solvation models. The predictions unambiguously pointed to axial fluorine for all salts investigated, including those with simultaneous axial F and (N)Me. The calculations were followed by synthesis of the corresponding series of 4,4-diphenylpiperidinium

salts. These were evaluated by one- and two-dimensional NMR spectroscopy in $[\text{D}_6]\text{DMSO}$ to fully corroborate the axial disposition of the fluorine in each of the compounds. X-ray crystal structure determinations were likewise performed for the diphenyl-3-fluoro NH_2^+ and NMe_2^+ systems to substantiate axial-F. Comparison of the X-ray structures of the fluorinated and unfluorinated NMe_2^+ salts reveals that the fluorine resides axial in spite of substantial steric compression. While the charge-dipole phenomenon respon-

sible for the axial-F conformation in the parent protonated fluoropiperidinium compounds carries over to doubly alkylated salts, we show that it extends to molecular orientation in the packing of the unit cells in the solid state as well. Finally, using the computational methods that successfully motivated our synthesis and structural work, we have made predictions for a number of new structures and re-examined some parallel results reported by the Eliel group in the early 1970s. Although C–F \cdots H–N hydrogen bonds are reported to be weak and few in number, the CF \cdots HN charge-dipole orienting effect is a powerful directing force that matches the hydrogen-bond in both its energetic contribution and conformational consequences.

Keywords: 3-fluoropiperidines • charge-dipole interactions • conformational analysis • density functional calculations • fluorine • molecular modeling


Introduction

The dynamic properties of substituted cyclohexanes represent one of the cornerstones of conformational analysis. Mono-substituted analogues universally prefer a substituent to occupy the equatorial orientation, although the energy gap between equatorial and axial conformations can typically range from 0.5 to 5.0 kcal mol⁻¹ depending on the nature of the substituent and the medium.^[1] Occasionally claims are made to the contrary,^[2,3] but they correspond either to an organomercurial system^[3] or to error.^[4] Ordinarily, cyclohexanes with multiple substituents and ring-atom replacement by heteroatoms behave in a similar manner.^[5,6] One unusual exception is the family of *N*-protonated 3-fluoro- and 3,5-difluoropiperidines. In water these compounds exist almost exclusively with the fluorine atom(s) occupying an axial and diaxial orientation, respectively.^[7,8] The source of the ring inversion found for six-membered rings has been at-

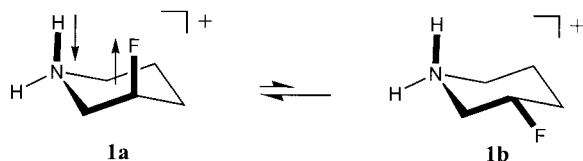
[a] Dr. A. Sun, Dr. K. Hardcastle, Dr. J. P. Snyder
Department of Chemistry, Emory University
Atlanta, GA 30322 (USA)
Fax : (+1)404-727-6586
E-mail: snyder@heisenbug.chem.emory.edu

[b] Dr. D. C. Lankin[†]
Pharmacia Corporation
4901 Searle Parkway, Skokie, IL 60077 (USA)
E-mail: lankindc@uic.edu

[[†]] New address: Medicinal Chemistry and Pharmacognosy College of Pharmacy, University of Illinois at Chicago College of Pharmacy, Chicago, IL, 60612-7231 (USA), Fax: (+1)312-996-7107

 Supporting information (1D and 2D NMR spectra for **6**; ¹³C data for model compounds; supplementary calculations for Scheme 1, and ESP map for structure **26**) for this article is available on the WWW under <http://www.chemeurj.org/> or from the author.

tributed to a four-center dipole–dipole interaction between parallel CF and NH bonds as in **1a**. Recently, we reported the operation of this effect in a molecule possessing a freely rotating CH₂F moiety.^[9]



In the present work, we examine the proposition that replacement of (NH₂)⁺ with (NMe₂)⁺ provides chair piperidines in which the axial fluorine survives in spite of apparent steric congestion afforded by axial methyl and the short C–N ring bonds. The study is supported by results of density functional theory (DFT) predictions, chemical synthesis, and detailed one- and two-dimensional NMR spectroscopy and X-ray crystallographic analysis.

Results and Discussion

Preliminary predictions: That the fluorine atom(s) in protonated 3-fluoro- and 3,5-difluoropiperidines prefer to occupy an axial orientation was first predicted from the results of molecular modeling. Both molecular mechanics (MM) and quantum-mechanical methods (QM) unambiguously forecast that the population of the F-axial conformer would strongly dominate the equilibrium between the interconverting chair piperidines in both the gas phase and aqueous solution. Follow-up synthesis and NMR evaluation of the equilibrium positions of a number of analogues fully confirmed

these earlier predictions.^[7,8] Table 1 displays typical results for the protonated 3-fluoropiperidine **1** using the 6–311G(d,p) basis set supplemented with DFT (Becke3LYP), MP2 correlation or a continuum solvation model (H₂O). In all cases, the axial fluorine conformer **1a** is estimated to show a population above 99% as observed. By comparison, fluorocyclohexane in solution sustains an equatorial/axial ratio in the range of 65:35 depending on the solvent.^[10] Subsequent investigations involving molecular modeling of the conformational profile of an acyclic variant possessing the NH/FC charge–dipole interaction was likewise substantiated in all details by extensive NMR experiments.^[9]

Accordingly, we considered a similar strategy to evaluate the hypothesis that a cationic axial *N*-methyl group in piperidine **2** is sufficiently polar to induce fluorine at C-3 to prefer an axial orientation. The intuitive basis for this expectation resides in the computational fact that *N*-methyl groups with a formal charge on nitrogen redistribute that charge primarily to the hydrogen atoms of the methyl group when evaluated by quantum-chemical methods.^[11,12] We surmised that the residual charge on hydrogen in the axial methyl group of **2** would provide sufficient electrostatic pulling power to induce the partially negatively charged fluorine to occupy a position of closest proximity; that is, F-axial **2a**. The equatorial form **2b** sacrifices the electrostatic attraction

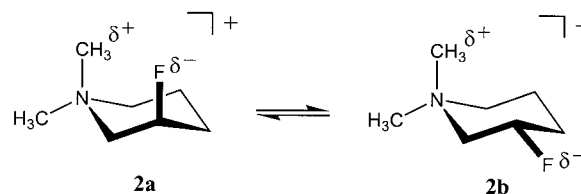


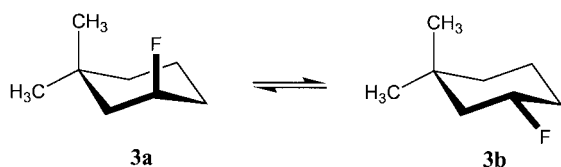
Table 1. Absolute and relative energies for axial and equatorial conformers of piperidines and salts derived from DFT, MP2, and MMFF calculations with and without a continuum solvation model.^[a]

	basis 1 ^[b]	ΔE_{rel} (%)	$E(\text{abs})$ [au] and $\Delta E(\text{rel})$ [kcal mol ⁻¹] (pop %)		basis 3 ^[d]	ΔE_{rel} (%)	MMFF/H ₂ O ΔE_{rel} (%) ^[e]
			basis 2 ^[c]	ΔE_{rel} (%)			
1a	–351.615 82	0.0 (99.99)	–351.720 43	0.0 (99.5)	–350.735 09	0.0 (99.6)	0.0 (99.6)
1b	–351.607 28	5.4 (0.01)	–351.715 50	3.1 (0.5)	–350.729 97	3.2 (0.4)	3.3 (0.4)
2a	–430.256 49	0.0 (99.9)	–430.341 10	0.0 (97.6)	–429.103 65	0.0 (97.2)	0.0 (99.5)
2b	–430.250 05	4.0 (0.1)	–430.337 56	2.2 (2.4)	–429.100 28	2.1 (2.8)	3.1 (0.5)
4a	–813.602 10	0.0 (99.95)	–813.692 74	0.0 (100)			0.0 (99.8)
4b	–813.594 89	4.5 (0.05)	–813.691 97	9.8 (0.0)			3.8 (0.2)
5a	–852.920 02	0.0 (99.95)	–852.985 04	0.0 (99.3)			0.0 (99.7)
5b	–852.912 80	4.5 (0.05)	–852.980 72	2.9 (0.7)			3.4 (0.3)
6a	–892.227 64	0.0 (99.8)	–892.297 33	0.0 (99.7)			0.0 (99.7)
6b	–892.221 73	3.7 (0.2)	–892.291 77	3.5 (0.3)			3.4 (0.3)
11a	–852.528 97	1.8 (4.6)	–852.534 34	0.7 (23.5)			0.3 (37.6)
11b	–852.531 96	0.0 (95.4)	–852.535 46	0.0 (76.5)			0.0 (62.4)
18a	–390.558 52	0.91 (17.7)	–390.561 52	0.4 (33.0)	–389.446 22	0.5 (30.1)	0.1 (45.8)
18b	–390.559 98	0.0 (82.3)	–390.562 18	0.0 (67.0)	–389.446 96	0.0 (69.9)	0.0 (54.2)
19a	–390.940 79	0.0 (99.5)	–391.010 65	0.0 (95.1)	–389.897 28	0.0 (96.0)	0.0 (94.4)
19b	–390.932 32	5.3 (0.01)	–391.006 31	2.7 (1.0)	–389.892 69	2.9 (0.7)	3.6 (0.2)
19c	–390.935 64	3.2 (0.5)	–391.007 61	1.9 (3.9)	–389.894 17	2.0 (3.3)	1.0 (5.4)
19d	–390.928 61	7.6 (0.0)	–391.002 37	5.2 (0.02)	–389.889 30	5.1 (0.02)	4.9 (0.02)

[a] Compounds **4a/4b**, **5a/5b**, and **6a/6b** are conformers of compounds **12**, **13**, and **14**, respectively. [b] Becke3LYP/6–311G(d,p)//Becke3LYP/6–311G(d,p) except for the diphenyl analogues **4–6** and **11** which employ Becke3LYP/6–31G*/MMFF/GABA/H₂O. [c] Becke3LYP/6–311G(d,p)/PCM//Becke3LYP/6–311G(d,p)/PCM except for diphenyl analogues **4–6** and **11** which employ Becke3LYP/6–31G*/PCM/MMFF/GABA/H₂O. [d] MP2/6–311G(d,p)//Becke3LYP/6–311G(d,p). [e] MMFF/GBSA/H₂O.

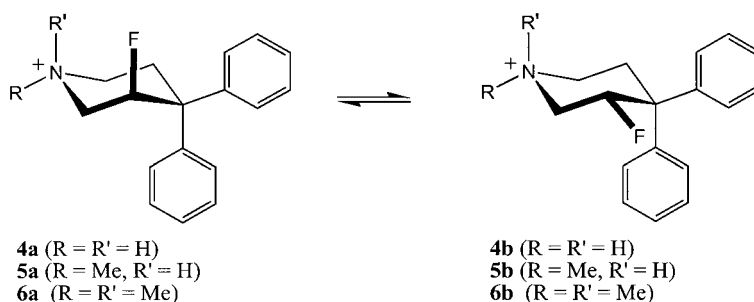
by placing the oppositely charged centers at a much greater distance.

Such attraction is, of course, offset by the close approach of two axial substituents in the six-membered ring. The cyclohexane A-value for methyl is substantial (1.74 kcal mol⁻¹), whereas that for fluorine is considerably less (0.25–0.42 kcal mol⁻¹) but still positive.^[10] The values together signal a significant steric effect between axially disposed F and Me and imply that axial fluorine in 3,3-dimethylfluorocyclohexane, **3**, will be disfavored relative to the equilibrium position in fluorocyclohexane. NMR measurements for **3** in CS₂ at -85 °C reveal an 0.64 kcal mol⁻¹ free energy difference between axial and equatorial conformers corresponding to a population of 85% for equatorial **3b**.^[13] While the halogen atoms (Cl, Br, and I) in the



other 3,3-dimethylhalocyclohexanes are sufficiently bulky to reveal no trace of the axial isomer by NMR spectroscopy, the F...Me steric effect is surprisingly diminutive. Relative to fluorocyclohexane, the presence of an axial methyl group increases the conformational free energy by only 0.34 kcal mol⁻¹ and decreases the axial population by just 15–25%. This can be understood by a comparison of the van der Waals radii. The fluorine vdw radius (1.47 Å)^[14] is only 23% larger than that of hydrogen (1.20 Å), whereas that for chlorine (1.75 Å) is expanded by 46%. Nevertheless, the conformational equilibrium in **3** overwhelmingly favors the equatorial conformer. Since the C–N bonds in the piperidinium salt **2** are approximately 0.06 Å shorter than their C–C counterparts in **3**,^[15,16,17] the 1,3 diaxial steric component of the total molecular energy for the former is expected to drive the equilibrium even further in the direction of the equatorial form.

With these considerations as background, we performed calculations for **2a** and **2b** as well as for the 4,4-diphenyl analogues **4** and **5**. Specifically, the conformers of **2** were optimized



with the density functional Becke3LYP/6-311G(d,p) protocol both in the gas phase and in “water” using the polarized continuum model of Tomasi and co-workers^[18] and reevaluated for energy using MP2 correlation. Similar to the results for **1**, the F-axial conformation is predicted to dominate at > 99%.

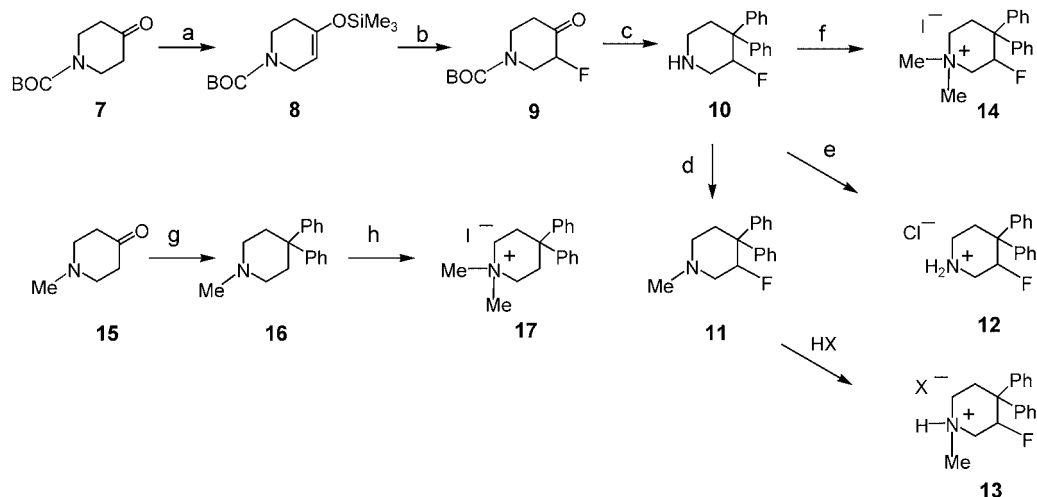
Structures **4–6** are too large for full DFT or ab initio optimization. Therefore, they were optimized with the MMFF force field^[19] coupled to a continuum water model and employed in subsequent single point DFT calculations (Becke3LYP/6-31G*). Again both protio and methyl analogues are posited to present axial-F (**4a–6a**) at the >99% population level (Table 1). Interestingly, the MMFF/GBSA/H₂O force field provides a very similar account of energies and populations for **1** and **2**. These molecular mechanics and quantum-chemical calculations motivated the synthesis and spectroscopic measurements described below.

Experimental justification for using the MMFF structures in this context is documented in Table 2 and constitutes comparison with the corresponding X-ray structures to be discussed below. For the NH₂⁺ system **4a**, the (N)H...F distances determined by MMFF and X-ray structural analysis are identical (2.60 Å). Similarly, the C–N and C–F bond

Table 2. Selected distances and angles for piperidines and salts^[a] derived from Becke3LYP/6-311G**^[b] and MMFF/GABA/H₂O optimization^[c] and X-ray crystallography.^[d]

	Distances [Å]		θ [°] (X)CCF	φ [°] XC–CF	φ [°] ^[e] RX...CF	θ [°] MeXC	φ [°] MeX–CC
	(N)H...F	(XC)H...F					
1a	2.311	–	104.8	60.2	1.7	60.2	1.7
1b	3.993	–	105.4	175.3	127.4	175.3	127.4
2a	–	2.220	108.5	70.8	0.2	70.8	0.2
2b	–	4.073	104.6	174.5	125.8	174.5	125.8
3a	–	2.359	109.5	71.3	–1.3	71.3	–1.3
3b	–	4.177	108.3	175.8	124.1	175.8	124.1
4a/12 ^[d]	2.602	–	106.9	60.6	–7.2	–	–
4a'	2.468	–	106.4	59.2	–3.8	–	–
4b'	–	4.046	108.4	–176.8	120.8	–	–
6a/14 ^[d]	–	2.223	109.1	67.9	–4.4	111.2	–74.6
6a'	–	2.260	107.5	67.5	–3.9	111.6	–75.0
6b'	–	4.078	107.9	177.9	117.5	111.2	–74.6
11 ^[d]	–	–	108.3	65.0	–124.5	110.8	177.5
11'	–	–	106.9	65.6	–122.1	110.3	178.3
18a	–	–	108.9	69.1	–111.4	111.7	176.4
18b	–	–	108.2	178.0	–15.4	112.0	172.9

[a] Compounds **4a/4b** and **6a/6b** are conformers of compounds **12** and **14**, respectively. [b] Basis set 2, Table 1. [c] Structures marked with a prime (e.g. **4a'**) are force-field optimized. [d] Structures determined by X-ray crystallography. [e] Improper torsions: Me–X...C–F or H–X...C–F, where X = N, C.



Scheme 1. Synthesis of **10–14**. a) TMSCl, Et₃N, DMF; b) Selectfluor, CH₃CN; c) TfOH, C₆H₆; d) CH₃I, NaHCO₃; e) HCl (g), CHCl₃; f) CH₃I, KOH, acetone; g) TfOH, C₆H₆; h) CH₃I, CH₂Cl₂.

lengths are within 0.01 Å, whereas bond angles around the C–F bond are within one degree. The cationic NHMe analogue **5a** likewise shows excellent geometric agreement between modeled and crystallographic structures (Table 2).

Synthesis: Although we have analyzed the problem of 3-fluoropiperidine conformation in terms of a minimally substituted ring, we have elected to utilize the 4,4-diphenyl series in the present investigation. Not only are these compounds easily synthesized, but interpretation of 2D NMR spectra and production of crystals for X-ray analysis are greatly simplified. Preparation of the target 3-fluoro-4,4-diphenylpiperidines **10–14** was initiated from the commercially available Boc-protected piperidone **7** (Scheme 1). Using literature procedures of the Terlings Park group,^[20] fluorinated intermediate **9** was prepared in two steps in 85 and 70% yields, respectively. Fluorinated diphenylpiperidine **10** was obtained as a colorless oil (85%) by TfOH-catalyzed double electrophilic addition to benzene using the procedure developed by Klumpp et al.^[21] Protonation and methylation provided salts **12–14** and the neutral piperidine **11**. Compounds **11**, **12**, and **14** were crystallized to provide samples suitable for X-ray crystallographic analysis (see below). The *N*-methyl protonated salt **13** was not isolated but generated by protonation in situ for analysis by NMR spectroscopy.

To compare fluorinated and unfluorinated salts, piperidine **16** was generated directly from commercially available 4-piperidone **15** by the same procedure used for the preparation of **10**. Methylation provided the iodide salt **17**, which was subjected to X-ray crystallographic analysis.

Determination of the structure and conformation in [D₆]DMSO solution by NMR spectroscopy: The solution structures of piperidinium salts **12** and **14** as well as the protonated form (CF₃COOD) of the free base **11**, namely **13**, were confirmed by extensive one- and two-dimensional

NMR (¹H/¹³C/gCOSY/gNOESY/gHSQC/gHMBC) investigations in [D₆]DMSO. The results presented in Tables 3–6 summarize the ¹H and ¹³C chemical shift assignments, the ¹H, ¹H, and ¹H, ¹⁹F coupling constants, and the ¹⁹F chemical shifts, respectively. The assignment strategy for this series of compounds involved: 1) complete assignment of the protons for each of the piperidines **12–14** using gCOSY, which provides information about proton coupling networks, and gNOESY (Figure 1), which affords information about spatial relationships (stereochemistry) via the nuclear Overhauser effect; 2) use of the one-bond C,H correlation experiment (gHSQC) for assignment of the protonated carbon atoms in each of the piperidines, and 3) use of gHMBC for obtaining H,C correlations two and three bonds away. Careful evaluation of all of the measured coupling constants (Table 5) and stereochemical information derived from the gNOESY ex-

Table 3. ¹H chemical shift assignments for diphenylpiperidinium salts **12**, **13**, and **14** and free base **11**; [D₆]DMSO, 25 °C, ppm.^[a]

Proton	NH ₂ ⁺ (12)	NHMe ⁺ (13)	NMe ₂ ⁺ (14)	NMe (11)
H-2 _{ax}	3.145 dd	3.357 dd	3.598 dd	[b]
H-2 _{eq}	3.607 t	3.909 t	4.074 t	[b]
H-3	6.287 br.d	6.436 br.d	6.426 br.d	5.861 d
H-5 _{ax}	2.513 t	2.526 t	2.588 t	[b]
H-5 _{eq}	3.056 d	3.217 d	3.196 d	[b]
H-6 _{ax}	2.699 t	2.865 t	3.100 t	[b]
H-6 _{eq}	3.263 d	3.494 d	3.676 d	[b]
H-2',6'	7.405 dd	7.416 dd	7.427 dd	7.365 dd
H-3',5'	7.303 t	7.306 t	7.313 t	7.249 t
H-4'	—	7.164 tt	7.164 tt	7.175 tt
H-2'',6''	7.423 dd	7.502 dd	7.504 dd	7.399 dd
H-3'',5''	7.367 t	7.379 t	7.371 t	7.269 t
H-4''	7.234 tt	7.243 tt	7.248 tt	7.126 tt
N-Me	—	2.800 s	3.255 s (eq) 3.123 s (ax)	2.092 s

[a] All assignments were confirmed by 2D NMR (gCOSY, gNOESY, gHSQC, gHMBC) experiments. [b] Shifts from 2.02–2.90 ppm broadened presumably by proton exchange.

Table 4. ^{13}C chemical shift assignments and $^nJ_{\text{C,F}}$ for diphenylpiperidinium salts **12**, **13**, and **14** and free base **11**; $[\text{D}_6]\text{DMSO}$, 25 °C, ppm.^[a]

Carbon	NH_2^+ (12)	NHMe^+ (13)	NMe_2^+ (14)	NMe (11)
C-2	43.0	52.8	60.3	55.1
	$^2J_{\text{C,F}}=21.0$	$^2J_{\text{C,F}}=20.7$	$^2J_{\text{C,F}}=19.3$	$^2J_{\text{C,F}}=20.2$
C-3	88.0	89.1	89.4	90.9
	$^1J_{\text{C,F}}=174.5$	$^1J_{\text{C,F}}=173.6$	$^1J_{\text{C,F}}=175.8$	$^1J_{\text{C,F}}=173.8$
C-4	46.8	46.5	46.5	47.4
	$^2J_{\text{C,F}}=19.8$	$^2J_{\text{C,F}}=20.2$	$^2J_{\text{C,F}}=19.9$	$^2J_{\text{C,F}}=17.9$
C-5	25.3	26.3	23.9	29.8
C-6	39.7	50.4	58.6	51.0
C-1'	144.3	144.5	143.8	144.2 br
C2',6'	125.8	126.4	126.5	126.8
C3',5'	128.4	128.6	128.6	128.1
C-4'	126.2	126.4	126.5	125.7
C-1''	141.5	141.3	141.2	144.4 br
	$^3J_{\text{C,F}}=6.7$	$^3J_{\text{C,F}}=7.0$	$^3J_{\text{C,F}}=7.2$	
C2'',6''	126.5	126.7	126.6	127.1
C-3'',5''	129.1	129.4	129.4	128.5
C-4''	126.8	127.0	127.1	126.0
N-Me	–	42.5 (eq)	56.6 (eq) 51.1 (ax), $J_{\text{C,F}}=6.5$	45.3 (eq)

[a] All assignments were confirmed by 2D NMR (gCOSY, gNOESY, gHSQC, gHMBC) experiments.

Table 5. ^1H , ^1H , and ^1H , ^{19}F coupling constants for diphenylpiperidinium salts **12**, **13**, and **14**; $[\text{D}_6]\text{DMSO}$, 25 °C, Hz.

$J(\text{H,H})$ or $J(\text{H,F})$	NH_2^+ (12)	NHMe^+ (13)	NMe_2^+ (14)
$^2J(\text{H,H})$			
$^2J_{2\text{ax},2\text{eq}}$	–14.4	–13.8	–14.5
$^2J_{5\text{ax},5\text{eq}}$	–16.1	–15.0	–16.3
$^2J_{6\text{ax},6\text{eq}}$	–13.0	–11.3	–13.6
$^3J(\text{H,H})$			
$^3J_{5\text{ax},6\text{ax}}$	12.6	12.5	12.4
aromatic rings			
$^3J_{2',3'}=^3J_{6',5'}$	8.3	8.2	8.2
$^3J_{4',3'}=^3J_{4',5'}$	8.3	8.2	8.2
$^4J_{2',4'}=^4J_{6',4'}$	1.6	1.6	1.6
$^3J_{2',3'}=^3J_{6',5'}$	8.3	8.2	8.2
$^3J_{4',3'}=^3J_{4',5'}$	8.3	8.2	8.2
$^4J_{2',4'}=^4J_{6',4'}$	1.6	1.6	1.6
$^2J(\text{H,F})$ or $^3J(\text{H,F})$			
$^2J_{\text{H-3,F}}$	42.9	40.5	42.8
$^3J_{\text{H-2ax,F}}$	40.0	40.5	39.3
$^3J_{\text{H-2eq,F}}$	10.4	11.8	10.7
$^3J_{\text{H-2eq,F}}$	10.7	11.8	10.7

Table 6. ^{19}F chemical shifts for diphenylpiperidinium salts **12**, **13**, and **14**; $[\text{D}_6]\text{DMSO}$, 25 °C, ppm.^[a,b]

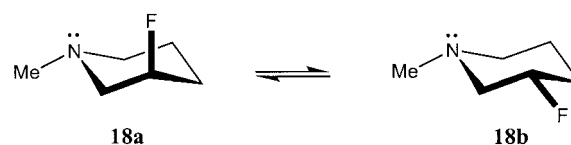
NH_2^+ (12)	NHMe^+ (13)	NMe_2^+ (14)
–193.8	–192.7	–190.1

[a] ^{19}F chemical shifts are expressed in ppm relative to external CF_3COOH (TFA) ($\delta = -76.4$ ppm) relative to CFCl_3 ($\delta = 0.00$ ppm). [b] The ^{19}F chemical shift for the free base of the N-Me compound in $[\text{D}_6]\text{DMSO}$ was observed at $\delta = -189.6$ ppm.

periments provides a complete solution structure for each of the fluoropiperidines. The ^1H NMR spectra (400 MHz) of piperidine salts **12**–**14** exhibited well-resolved proton signals associated with both the piperidine ring and the two distinctly different phenyl rings (axial and equatorial). Resolu-

tion of scalar J -coupling and spatial relationships attributed to the phenyl ring protons was crucial for derivation of an unequivocal and self-consistent set of assignments for all ^1H and ^{13}C signals in the diphenylpiperidine series.

An interesting feature of the ^{13}C chemical shifts for **11** and **13** relates to calculated charge distribution. As noted above, while the positive charge on ammonium salts is generally assigned intuitively to the more electronegative nitrogen atom, quantum-chemical charge calculations routinely show it to have preferentially migrated to the hydrogen atom of (N)H or to the protons of an N -methyl group ((NC)H₃) leaving both N and C partially negatively charged (see Figure 3 and S6 in the Supporting Information).^[11] ^{13}C NMR chemical shifts support this idea. For example, the (N)Me ^{13}C chemical shifts for neutral **11** and cationic **13** are found at $\delta = 45.3$ and 42.5 ppm, respectively; the methyl carbon atom of the cation is more shielded ($\Delta\delta = 2.8$ ppm) than the corresponding carbon atom in the neutral species. A similar relationship exists for carbon atoms C-2 and C-6 in the neutral and cationic systems yielding an average ^{13}C shielding of 1.9 ppm for the three carbon atoms bound to the N atom in the protonated salt (cf. Table 4 and Figure S6 in the Supporting Information). The NBO^[11,12] atomic charges at carbon bonded to nitrogen for Becke3LYP/6–311G(d,p) optimized structures of **18a** and the corresponding protonated cation **19a** are nearly equivalent with values of -0.35 , -0.22 , -0.18 and -0.34 , -0.20 , -0.16 , respectively (see Figure S6 in the Supporting Information). While the differences in the two sets of charges do not translate con-



veniently into ^{13}C chemical shifts, they do suggest that, if charges are a significant factor, then the shifts for the ammonium cation should be similar to those for the neutral amine as observed.

To put this analysis in perspective, we note that ^{13}C chemical shifts are not fully attributable to atomic charge accumulation. Unlike the diamagnetic shielding characterizing proton chemical shifts (σ^d), ^{13}C shifts are dominated by paramagnetic shielding (σ^p). The latter is composed of three contributions as expressed by the Ramsey–Karplus–Pople equation ($\sigma^p \approx (1/\Delta E) \langle 1/r^3 \rangle (\Sigma Q_{ij})$).^[22] The ΔE and ΣQ_{ij} terms correspond to electronic excitation to low-lying electronic states and π -bonding, respectively. Since saturated carbon, amines, and ammonium salts possess neither characteristic, the contributions are expected to be relatively small. The $\langle 1/r^3 \rangle$ contribution is a radial distribution term reflecting the average distance of 2p electrons from the nucleus. It parallels the inductive effect at protons, and given the electron-withdrawing effect of nitrogen, most likely makes the largest contribution in the present cases to the chemical shifts of C(N). Consequently, we regard it as plausible that the relative deshielding of the latter centers for **11** relative to **13**

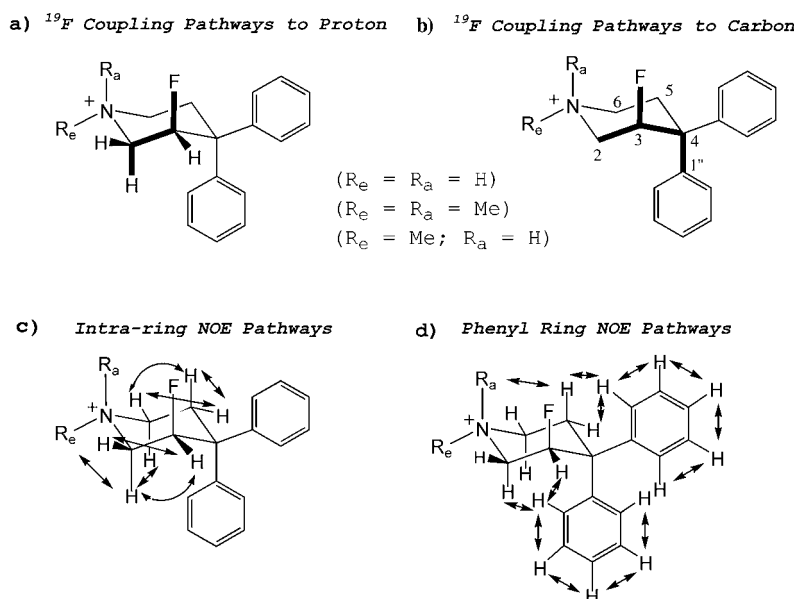


Figure 1. Scalar and cross relaxation pathways from NMR analysis of piperidines **12**, **13**, and **14**; a) $^3J_{\text{H,F}}$; b) $^3J_{\text{C,F}}$; c) piperidine ring NOE cross-peaks; d) NOE cross-peaks associated with the 4,4-phenyl rings.

owes its origin in large measure to the sizeable negative charge at nitrogen-bonded carbon in the ammonium cation.

The influence of the fluorine atom on the proton spectra of piperidines **12–14** provides a valuable marker for assessing structure and conformation. Characterized by ^{19}F spin-spin coupling (vicinal) to each of the equatorial and axial protons at C-2 of the piperidine ring and by spin-spin coupling to the proton at C-3 (geminal coupling, Figure 1a), the spectra are completely compatible with observations reported earlier for 3-fluoropiperidine hydrochloride **1a** in D_2O solution.^[7]

The fluorine atom also exhibits spin-spin coupling to carbon atoms in the immediate “local neighborhood” proximal to the fluorine (Figure 1b). Fluorine coupling to C-3 ($^1J_{\text{C,F}}$), C-2, and C-4 ($^2J_{\text{C,F}}$) and the *ipso*-carbon of the axial phenyl ring C-1'' ($^3J_{\text{C,F}}$) was observed for piperidines **12–14**. The latter assignments were rendered unequivocal on two counts. First, the proton signals originating from each of the phenyl rings were clearly observable, and second the axial and equatorial nature of each phenyl ring could be evaluated from a combined analysis of the gCOSY, gNOESY, gHSQC, and gHMBC two-dimensional NMR data. For the dimethylpiperidinium compound **14**, a long-range $^{13}\text{C},^{19}\text{F}$ coupling from the fluorine atom to the axial methyl group was also observed (6.5 Hz). This type of coupling, mediated by means of a through-space $\text{F}\cdots\text{H}$ interaction, has been observed in fluorinated steroid systems between an axial (beta) fluorine at C-6 and the angular methyl group at C-19.^[23]

The solution conformational profile for all three piperidinium salts **12–14** is consistent with an essentially exclusive axial fluorine atom located at C-3. This is clearly indicated by: 1) the large (40.5–42.9 Hz) vicinal $^3J_{\text{H,F}}$ coupling constant between the fluorine atom attached to C-3 and the axial

proton at C-2 for each of the salts (Table 5), 2) a large vicinal $^3J_{\text{H,H}}$ coupling constant (12.4–12.6 Hz) between axial protons at C-5 and C-6, and 3) the substantial coupling (6.7–7.2 Hz, Table 4) between the fluorine atom and the *ipso*-carbon atom C-1'' of the axial phenyl ring. With respect to 1), the maximum observed vicinal $^3J_{\text{H,F}}$ for an F-C-C-H dihedral angle of 180° (47–48 Hz) occurs in cyclohexanes.^[24,25] The somewhat reduced values observed for piperidinium salts **12–14** (40.5–42.9 Hz), the largest thus far observed for this type of $^3J_{\text{H,F}}$ coupling, result from attenuation by the electronegative charged ring nitrogen. Nonetheless, they correspond to a fully anti F-C-C-H dihedral angle as

predicted by a carefully parameterized Karplus relationship for $^3J_{\text{H,F}}$ for couplings.^[24] Thus, couplings 1)–3) in $[\text{D}_6]\text{DMSO}$ are consistent with a conformationally biased piperidinium system in which the equatorial conformers are populated to such a minimal extent that only the axial conformers make a significant contribution to the NMR spectra. They likewise conform in detail to the computational predictions that **12–14** exist as the axial conformers **4a–6a**, respectively, in polar solution (Table 1).

The axial and equatorial methyl groups bonded to the nitrogen atom in piperidine **14** are clearly differentiated by the gNOESY measurements. The axial methyl shows NOE cross peaks to the equatorial protons at C-2 and C-6, the axial proton at C-5, and the equatorial methyl group attached to the nitrogen atom. The latter displays NOE cross peaks to both axial and equatorial protons attached to C-2 and C-6 and to the axial *N*-methyl group. In protonated **11**, namely **13**, the methyl group bonded to the nitrogen atom exhibits NOE cross peaks only to the axial and equatorial protons at C-2 and C-6. No cross peaks were observed from the *N*-methyl group to the axial proton at C-5 strongly suggesting that protonation of **11** to give **13** occurs in an axial manner. This point is elaborated below in connection with calculations of the relative energies for the four isomers **19a–19c**.

The ^1H NMR spectrum of the neutral piperidine **11** was also investigated as a preliminary to generating its protonated form **13**. In both CDCl_3 and $[\text{D}_6]\text{acetone}$ (400 MHz, 25°C) although the aromatic and *N*-Me protons are sharp, the remaining ring protons (including the 2-H(CF)) are somewhat broad indicative of dynamic broadening. Raising the temperature of the sample to 50°C in the NMR spectrometer causes sharpening of the ring proton signals. Speculating that the latter was due to residual HI from *N*-meth-

ylation and/or HCl from deuterated chloroform, we stirred the CDCl_3 NMR sample with basic alumina, evaporated it to dryness, and took up the residue in C_6D_6 . The resulting ^1H NMR spectrum (25°C) proved to be sharp, well-resolved and nearly identical to the CDCl_3 spectrum recorded at 50°C . Slow equilibration between neutral **11** and a low concentration of its protonated form, **13**, appears to be responsible for the line broadening.

X-ray crystallography and charge distribution: Single-crystal X-ray structure determination has been carried out for piperidine **11** and piperidinium salts **12**, **14**, and **17**. The results are in complete accord with the present and previous^[7,8] NMR measurements, but for the first time structural details for the 3-fluoropiperidinium salts are available. Selected internal variables for **12** are depicted in Figure 2a. Most striking

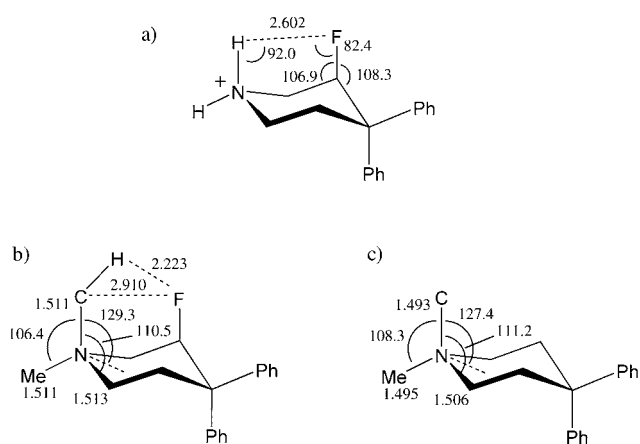


Figure 2. Selected internal variables from the X-ray structures of piperidinium salts; a) **12** (**4a**), the $\text{NH}\cdots\text{FC}$ local geometry; improper torsion $\varphi(\text{NH}\cdots\text{FC}) = 6.9^\circ$; b) **14** (**6a**), $(\text{N})\text{CH}\cdots\text{F}$ local geometry; improper torsion $\varphi(\text{N})\text{CH}\cdots\text{FC} = 40.6^\circ$; and c) **17**, local geometry around N^+Me_2 .

ing is the geometry around the $\text{NH}\cdots\text{FC}$ dipoles. The $\text{H}\cdots\text{F}$ separation at 2.60 \AA is clearly outside values ascribed to the usual hydrogen-bond, as are the $\text{N}\cdots\text{H}\cdots\text{F}$ and $\text{H}\cdots\text{F}\cdots\text{C}$ angles. The latter and the improper $\text{NH}\cdots\text{FC}$ torsion ($\varphi(\text{NH}\cdots\text{FC}) - 6.9^\circ$) do reflect, however, that the $\text{N}\cdots\text{H}$ and $\text{C}\cdots\text{F}$ bonds are nearly parallel and planar. The geometry is precisely that required for a strong dipole–dipole association accompanied by a charge–dipole component as illustrated by structure **1a** and Figure 3a. We note that although a dipole moment cannot be assigned to a charged molecule,

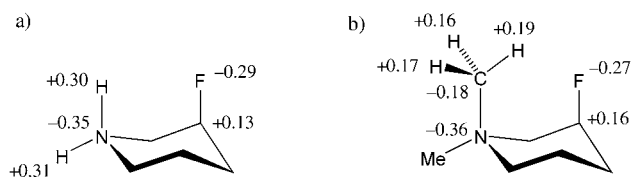


Figure 3. Mulliken charges obtained at the Becke3LYP/6-311G(d,p) level. a) **1a**; b) **2a**.

local intramolecular dipole–dipole interactions nonetheless operate. In the present case, the atomic charge calculations depicted in Figure 3a and Figure S6 in the Supporting Information suggests that the $\text{C}\cdots\text{F}$ and $\text{N}\cdots\text{H}$ bond dipoles are of similar magnitude. A more graphic illustration compares the electrostatic potential energy surface of conformational isomers **1a** and **1b** in Figure 4. The F-axial form clearly brings two charge-complementary surfaces together.

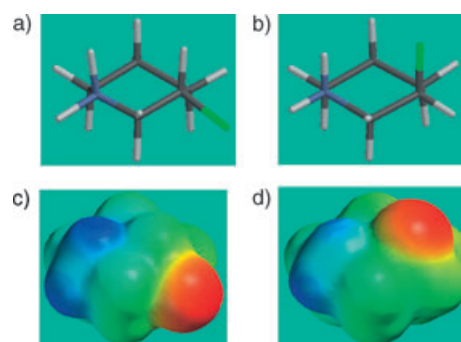


Figure 4. Chair conformers of piperidinium salt **1** (Becke3LYP/6-311G(d,p) optimized) complemented by HF/6-31G(d,p) electrostatic potential surfaces; blue corresponds to regions of strong positive charge, while red reflects strong negative charge; a) and c) equatorial **1b**; b) and d) axial **1a**.

Within the Becke3LYP/6-311G(d,p)/PCM solvation model, the axial isomer **1a** is less solvated than equatorial **1b** by $3.6 \text{ kcal mol}^{-1}$, a number slightly higher than that previously derived by AMSOL calculations.^[7] In water, although the equatorial form is computed to be more stabilized by solvation, the axial form persists with an advantage of at least $2.5 \text{ kcal mol}^{-1}$ based on the lack of observation of the equatorial form by NMR spectroscopy or X-ray crystallography. Accordingly, the intramolecular $\text{NH}\cdots\text{FC}$ interaction is suggested to amount to $>4\text{--}6 \text{ kcal mol}^{-1}$, a quantity generally associated with another more familiar type of non-covalent interaction; namely, a reasonably strong hydrogen bond.

A similar analysis for the fluorodimethylpiperidinium salts **2a** and **2b** likewise indicates the equatorial isomer to be favored by solvation in the PCM aqueous continuum model; $\Delta\Delta G_{\text{sol}}(\text{eq}\text{--}\text{ax}) = -2.0 \text{ kcal mol}^{-1}$. Nonetheless only F-axial **6a/14** is observed both in solution and in the solid state. For **1a**, with the $(\text{N})\text{H}\cdots\text{F}(\text{C})$ separation at the van der Waals boundary (2.60 versus 2.67 \AA , the sum of F (1.47) and H (1.20) radii),^[14] the axial halogen is a balance between coulombic and solvation forces. For dimethyl compound **2a**, the situation appears to be a bit more complicated, since 1,3-diaxial repulsion effects would appear to be involved as well. Figure 2b illustrates that for **6a/14** the $\text{H}\cdots\text{F}$ separation of 2.22 \AA is 0.45 \AA below the sum of the van der Waals radii, as is the $\text{C}\cdots\text{F}$ distance of 2.91 \AA ($\text{vdW sum} = 3.17 \text{ \AA}$; $\Delta r = 0.26 \text{ \AA}$). The crowding is manifested by subtle but coordinated atom movements in the molecule. Comparison with the unfluorinated dimethyl salt **17** provides a measure of the effect. Figure 2b and c illustrate that the NMe_2 group and

the C–F bond in **6a/14** have retreated from one another. Thus, the Me–N–Me angle is diminished, whereas the C–N–Me and Me–N–centroid angles are enlarged in **17** relative to those in **14** reflecting the backward movement of the axial *N*-methyl group. Similarly, fluorine backpedaling in **6a/14** is indicated by the slight reduction in the C4–C–F bond angle relative to that in **12** (Figure 2a). Accompanying these angular deformations, slight stretching of the N–Me and C–F bonds is observed in **6a/14**. Although each individual structural variation in the latter is small, the cumulative changes make it clear that the compacted F and Me atoms are attempting to minimize 1,3-diaxial steric repulsion. It is important to add that the relative errors in the bond lengths and angles, ~0.008 Å and 0.5°, respectively, are well below the deformations noted above.

Remarkably, the combination of solvation favoring the F-equatorial conformation and the repulsive elements inherent in the F-axial conformer are insufficient to favor the F-equatorial form for **6a/14** in either solution or the solid state. The short intramolecular distances (Figure 2b) and complementary electrostatic forces shown in Figure 3b appear to be the source of conformational preference. While calculated partial charges are well known to arise as a consequence of the partitioning scheme,^[26] the depicted values nonetheless reflect the distribution expected for a significant Me...F attraction as well as charge polarization in the methyl group to maximize the interaction.^[11] A very similar set of partial charges obtain for the MMFF optimized structure **4a** evaluated as a single point at the Becke3LYP/6–31G* level (Table 1). Within the PCM aqueous continuum model, the charges shown in Figure 3 are attenuated by 5–10% for **4a**, but otherwise present the identical picture. A somewhat different distribution would arise by including explicit water molecules in the calculation, although it will certainly offer the same qualitative description.

Finally, we have also obtained the X-ray crystal structure of the neutral fluorinated piperidine **11**. Surprisingly, the compound displays an axial fluorine. Given that both NMR and the conformational analysis (Table 1) suggest that the two conformers exist side by side in a dynamic equilibrium, the molecule must enjoy stabilizing interactions with neighboring molecules in the solid state. The unit cell analysis presented below provides a clear basis for this viewpoint.

Interaction within the unit cells: Examination of the unit cells for the piperidine crystal structures reveals a number of interesting features. For compound **11**, the rings present as dimers as illustrated in Figure 5. Reminiscent of the methyl–fluorine interaction in **4a/12** (Figure 2b and Figure 3b), the fluorine is associated with C–H bonds adjacent to centers bearing electronegative atoms at distances just below the van der Waals sum (2.52–2.54 Å versus the vdW sum of 2.67 Å^[14]). It is difficult to distinguish whether the interactions in free amine **11** are energetically productive, or simply allowable. Nevertheless, the atomic associations are entirely consistent with observations described above and below.

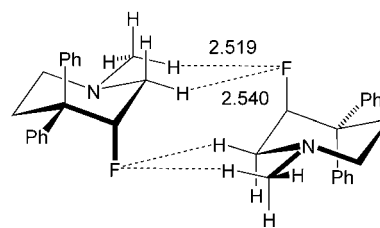


Figure 5. Chair CH...FC interactions in the X-ray crystal structure of **11**; H...F separations are given in Å.

Quaternary salts **4a/12** and **6a/14** evidence intermolecular contacts very similar to those observed intramolecularly for **6a/14**. The latter, for example, presents a pair of CH bonds adjacent to the nitrogen center in a chelating type arrangement with fluorine as shown in Figure 6a. The H...F separa-

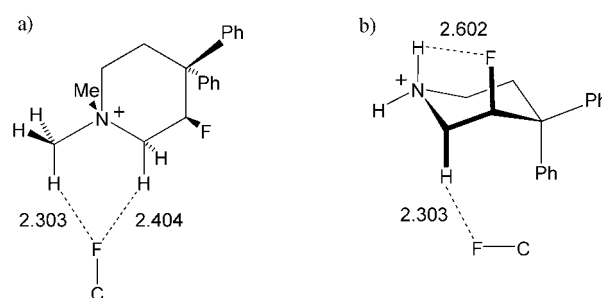
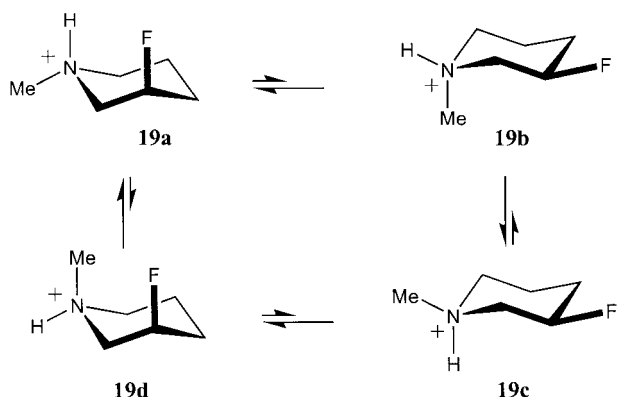


Figure 6. Intermolecular CH...FC interactions in the X-ray crystal structures of **6a/14** (a) and **4a/12** (b); H...F separations are given in Å.

tions are well below the van der Waals radii, and the 2.3–2.4 Å separations are only 0.08–0.18 Å longer than the corresponding intramolecular distances. It is safe to conclude that the forces between molecules in the crystal are not benign, but provide association energies of the same order of magnitude as that sustained by NMe and F in the same molecule. Surprisingly, protonated **4a/12** does not involve NH...FC association in the crystal, but shows NCH...FC encounters instead (Figure 6b). Apparently, the diaxial intramolecular forces are sufficiently strong to damp cross-molecule interactions at the NH₂⁺ center in the crystal. Again the intermolecular distances are identical to those observed in **6a/14** with presumably the same consequences for crystal stability.

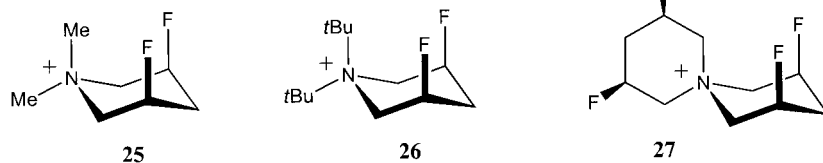
Further possible examples of the charge–dipole effect: The predominance of axial fluorine in **6/14** makes it clear that the CF...MeN⁺ interaction is significant. This raises the question as to whether there is an effective competition between the latter and the CF...HN⁺ interaction in **5/13**. X-ray and NMR analyses for the compound allow the conclusion that the piperidine ring sustains a *trans*-diaxial interaction between fluorine and the C2 vicinal proton. However, no information has been forthcoming regarding the simultaneous axial disposition of both the *N*-methyl group and the fluorine atom in **5/13**, that is, **19d**.

The issue has been examined by evaluating the four conformers **19a–19d** with DFT/H₂O supplemented by single point MP2/H₂O calculations (Table 1). The form with F-



axial and methyl group equatorial, **19a**, is the global minimum with a predicted population of 95–96% in agreement with the X-ray structure for **5a**. However, the axial–axial conformer **19d** is posited to participate in the equilibrium at 298 K with a population of 3–4%. The A-value for methylcyclohexane (1.75 kcalmol⁻¹)^[10] corresponds to the same population for the axial-methyl group conformation. The relatively short N–C bond lengths in the ring most certainly occasion steric repulsion as described for **6a/14** (Figure 2). Yet the double axial system **19d** compensates electrostatically such that the energy penalty amounts to only that of a single axial methyl in cyclohexane. In an effort to obtain experimental verification of the presence of the conformation represented by **19d**, the gNOESY spectrum of **13** was carefully examined for a cross peak between the *N*-methyl group and the axial proton at C-5. If such a cross-peak is present, it proved too weak to observe. Finally, the F-equatorial isomers **19b** and **19c** are estimated to contribute <1% to the dynamic equilibrium.

Three additional structures, **25–27**, appeal to us as interesting synthetic targets that would extend the principles described in this work. Both **25** and **26** can, in principle, exist as triaxial and axial-di-equatorial conformers in solution.



Using the solvent-based methods described above (e.g. Becke3LYP/6–31G*/PCM/H₂O//MMFF/GABA/H₂O), we predict that the triaxial forms will predominate with predicted populations of >99 and 54% (298 K), respectively. The nearly 50:50 population for axial and equatorial isomers of di-*tert*-butyl compound **26** is surprising. Like **6a/14**, the axial isomer is crowded with predicted F...H distances ranging from 2.1–2.3 Å (cf. Figure 2). However, the axial *tert*-butyl group for the optimized structure is not symmetrically dis-

posed above the ring plane. It rotates one of its methyl groups to provide maximal interaction with only one of the two axial F atoms. Once again electrostatic F...H interaction appears responsible for the predicted outcome. As is well-known, calculated atomic charge distribution alternates down a chain of atoms. In **26**, the 6–31G(d,p) natural (NBO) charges^[11] for the chain N–C(ax-*t*Bu)–C–H varies as follows: –0.32, +0.16, –0.71, +0.24 (+0.26, +0.27). The corresponding Mulliken charges on the protons of the CH₃ group near the axial F atoms are +0.14, +0.15, and +0.19. As a result, the coulombic interactions between the *t*Bu group and the axial F atom (–0.42 (NBO), –0.39 (Mulliken)) in **26** are of the same order of magnitude as for axial **6a/14** (cf. Figure 3). Figure S5 in the Supporting Information provides an illustration of the *t*Bu methyl group...ax-F attraction similar to that shown in Figure 4 and Figure 7.^[27] Thus, in spite of the severe axial crowding, a significant pop-

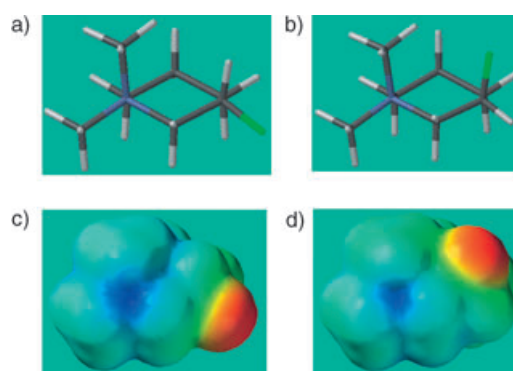


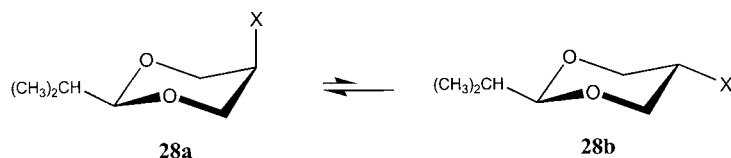
Figure 7. Chair conformers of dimethylpiperidinium salt **2** (Becke3LYP/6–311G(d,p) optimized) complemented by HF/6–31G(d,p) electrostatic potential surfaces; blue corresponds to regions of strong positive charge, while red reflects strong negative charge; a) and c) equatorial **2b**; b) and d) axial **2a**.

ulation of the diaxial fluorine conformation is predicted. Structure **27** can sustain three chair piperidine conformations for the fluorine pairs: ax–ax, eq–ax, and eq–eq. These are prognosticated to equilibrate with populations of >99, <0.01, and <0.01% (298 K), respectively.

Finally, while this work and its recent precursors^[7,8,9] focus exclusively on the conformational properties of fluoropiperidines, it is not the first effort to take advantage of electrostatic effects to tip the balance in favor of axial orientation in six-membered rings. Substitution of cyclohexanol and its benzoate with electronegative groups at C-4 elicits eq/ax ratios from 49/51 to 26/74 at low temperatures.^[28] Piperidine salts with RO, Br, and F at C-4 provide a similar spread for eq/ax conformers.^[29,30] Dimethylpiperidinium ions with OH and OAc at C-3 were reported to give eq/ax ratios of 49/52 and 34/66, respectively, in perdeuteromethanol.^[28] These

ratios correspond to a relative stabilization of the axial conformer by 0.1–0.8 kcal mol⁻¹. Even more striking is the position of the acid-catalyzed chemical equilibrium in substituted dioxolanes **28** reported in a series of publications by the Eliel group.^[31]

Of particular relevance to the present work are the charged substituents X = Me₂S⁺, NH₃⁺, NHMe₂⁺, and NMe₃⁺ all of which were shown to exist as **28a**. The latter was deter-



mined to be more stable than **28b** by >2.0 kcal mol⁻¹ corresponding to an axial population of >97% at 298 K in various polar carboxylic acid solvents. To examine the consistency of these results with our own, we have modeled the configurational diastereomers of **28** for X = NH₃⁺ and NMe₃⁺ with the Becke3LYP/6311G(d,p)/PCM//MMFF/GABA/H₂O protocol. Both ammonium substituents are predicted to favor the axial form **28a** by 4–6 kcal mol⁻¹ in agreement with observation. The optimized structures are fully compatible with those derived for the piperidines (Figure 8). Specif-

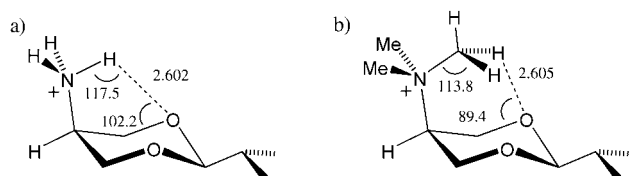


Figure 8. Selected internal variables from MMFF/GBSA/H₂O optimization of Eliel and Alcudia's axial dioxanes; a) **28a** (X = NH₃⁺) the NH...OC local geometry; the improper torsion $\varphi(\text{NH}\cdots\text{OC}) = 5.6^\circ$; b) **28a** (X = NMe₃⁺) the (NC)H...OC local geometry; the improper torsion $\varphi(\text{NCH}\cdots\text{OC}) = 62.6^\circ$.

ically, for **28a** (X = NH₃⁺) the calculated NH...O distance of 2.60 Å is very similar to that derived for the NH...F separations in **1a**, **4b/12**, and **5a/13** (2.60 Å, Figure 2). Likewise, the closest (NCH₂)H...O distance in **28a** (X = NMe₃⁺) is 2.61 Å, slightly longer than the (NCH₂)H...F separation in **14** and **19c** (2.22 Å). Equally important are the dipole orientations. As with the piperidines discussed above, the NR and CO bonds do not satisfy the classical hydrogen bonding geometries, instead conforming to a favorably oriented charge–dipole or dipole–dipole interaction. In **12/4a** and **28a** (X = NH₃⁺) the improper torsions $\varphi(\text{NH}\cdots\text{XC})$ are 6.9 and 5.6°, respectively, whereas the bond angles around the NH and XC centers (X = F and O) are similar (cf. Figure 2 and Figure 8). A comparison of the *N*-methylated systems **14/6a** and **28a** (X = NMe₃⁺) demonstrates a similar correspondence. In this pair of comparisons, the two parallel C–O bonds in the dioxane rings of **28** plays the same role as the single C–F bond in the fluoropiperidines.

Summary and Conclusions

Predictions based on density functional theory that 3-fluoropiperidine salts exist exclusively as the F-axial conformers have been substantiated by the synthesis of a series of 4,4-diphenyl analogues, detailed analysis of the conformation by NMR spectroscopy in D₂O and X-ray crystallography. Of particular importance is the finding that the *N,N*-dimethyl salt **14**, like its less encumbered NH₂⁺ and NHMe⁺ counterparts, was predicted and then established to likewise display axial-fluorine in solution and the solid state in spite of considerable diaxial steric compression. Short range CH...FC charge–dipole interactions mediated by positive charge accumulation at hydrogen atoms of the *N*-methyl groups are sufficient to counterbalance the latter. An overall energetic advantage for axial fluorine is estimated to be 4–6 kcal mol⁻¹, very similar to that of a strong hydrogen bond. The intramolecular phenomenon appears to be more general as illustrated by its intermolecular operation in the solid state for **11**, **12**, and **14** as well. The surprising appearance of axial fluorine in neutral **11** in the crystal is attributable to this source.

Three additional points are noteworthy. First, the use of the MMFF force field to optimize molecular geometries followed by single-point large basis set DFT and/or MP2 calculations provides energy differences that are equivalent to using a full quantum-chemical treatment throughout (cf. Table 1). This strategy should prove useful in evaluating larger structures that push the limits of computational resources. Second, the MMFF/DFT strategy has been applied to the analysis of a series of previously reported dioxolanes **28** that exhibit unusual conformational profiles. The charge–dipole effect in both its geometric and energetic manifestations carries over to such cyclic structures as it does to acyclic systems.^[9] The phenomenon is certainly general and likely to express itself broadly across biologically active small molecules^[32,33,34] and protein systems alike.^[35] In this context we have predicted that a series of highly crowded structures (**25–27**) should also conform to the F-axial paradigm.

Finally, while the conformational analysis of any number of substituted cyclohexanes and piperidines yields a mixture of rapidly equilibrating conformers,^[1,27,28,29] the 3-fluoropiperidine salts are satisfyingly “clean”. Yet the energy difference is certainly no more than 2–3 kcal mol⁻¹, a quantity attributable to a small but productive charge attenuated dipole–dipole interaction. It is conceivable that the overwhelming axial bias in 3-fluorinated piperidines can be used productively in organic synthesis. The substitution might be used to guide the regiochemistry of a synthetic reaction or to control product stereochemistry in the spirit of a chiral auxiliary. Subsequent reductive removal of fluorine would restore the unhalogenated heterocycle.

Experimental Section

General: Melting points were determined by using a Thomas–Hoover capillary melting point apparatus and are reported without correction. Mass spectrometric analysis was provided by the Emory University Mass Spectrometry Center. Routine proton and carbon NMR spectra measured during synthesis were obtained on Varian Inova-400 (400 MHz) or Varian Inova-600 (600 MHz) spectrometers. Solvent for NMR was deuteriochloroform with residual chloroform ($\delta = 7.26$ ppm for proton and $\delta = 77.7$ ppm for carbon) taken as internal reference and reported in parts per million (ppm). TLC and preparative thin-layer chromatography (PTLC) were performed on precoated, glass-backed plates (silica gel 60 F₂₅₄; 0.25 mm thickness) from EM Science and were visualized by UV lamp. Chromatography was performed with silica gel (230–400 mesh ASTM) or neutral alumina (80–200 mesh) from EM Science using the “flash” method.^[36] Elemental analyses were performed by Atlantic Microlab Inc. Norcross, Georgia. All solvents and other reagents were purchased from Aldrich Chemical Co., Milwaukee. The reagents were used as received. All reactions were performed under anhydrous nitrogen atmosphere in oven-dried glassware.

1-tert-Butoxycarbonyl-1,2,3,6-tetrahydro-4-(trimethylsilyloxy)pyridine (8):^[20] To a stirred solution of **7** (995 mg, 5 mmol) in dry DMF (5 mL) was added TMSCl (0.76 mL, 6 mmol) and then dry Et₃N (1.68 mL, 12 mmol). The mixture was stirred at 80 °C overnight (about 20 h), diluted with hexane, and washed with NaHCO₃ (3 × 5 mL). The organic layer was washed with brine and dried over Na₂SO₄. Purification by chromatography using hexane/EtOAc (9:1) as eluent gave **8** (1.15 g, 85%) as a colorless oil: ¹H NMR (400 MHz, CDCl₃): $\delta = 0.20$ (s, 9H), 1.45 (s, 9H), 2.15 (m, 2H), 3.52 (t, $J = 5.7$ Hz, 2H), 3.85 (m, 2H), 4.78 ppm (m, 1H).

1-tert-Butoxycarbonyl-3-fluoro-4-piperidone (9):^[20] Selectfluor reagent (3.9 g, 11 mmol) was added to a stirred solution of **8** (2.71 g, 10 mmol) in dry MeCN (100 mL) at 0 °C, warmed to room temperature for about 1.5 h, then poured into EtOAc (20 mL), washed with brine, and dried over Na₂SO₄. The product was first purified by chromatography using hexane/EtOAc (2:1) as eluent, then rechromatographed on alumina using MeOH/EtOAc (5:95) as eluent to give **9** (493 mg, 70%) as a colorless oil: ¹H NMR (400 MHz, CDCl₃): $\delta = 1.50$ (s, 9H), 2.48–2.60 (m, 2H), 3.20–3.27 (m, 2H), 4.18 (m, 1H), 4.44 (m, 1H), 4.84 ppm (m, 1H).

4,4-Diphenyl-3-fluoro-piperidine (10): TfOH (0.5 mL) was added dropwise to a stirred solution of **9** (10 mg, 46 μ mol) in dry benzene (0.5 mL). The solution was stirred at room temperature for 2.5 h, then poured into CHCl₃ (5 mL), washed with saturated NaHCO₃, dried over MgSO₄, concentrated in vacuo, and purified by chromatography with EtOAc/MeOH/Et₃N (3:1:0.01) as eluent. Compound **10** was obtained as a colorless solid (10.0 mg, 85%): m.p. 65–67 °C; ¹H NMR (600 MHz, CDCl₃): $\delta = 1.88$ (m, 1H), 2.51 (m, 2H), 2.78–2.82 (m, 1H), 3.00–3.04 (m, 1H), 3.14 (dd, $J = 14, 35$ Hz, 1H), 3.24–3.26 (m, 1H), 5.48 (m, 1H), 7.14–7.35 ppm (m, 10H); ¹³C NMR (600 MHz, CDCl₃): $\delta = 32.57, 42.43, 46.89, 46.90, 47.02, 47.04, 90.92, 92.09, 126.21, 126.46, 127.01, 127.30, 128.43, 128.90, 143.86, 143.90, 145.99$ ppm; MS (FAB⁺): m/z : 256.2.

N-Methyl-4,4-diphenyl-3-fluoro-piperidine (11): To a solution of 4,4-diphenyl-3-fluoropiperidine **10** (20 mg, 80 μ mol) in dry dichloromethane (2 mL) was added iodomethane (11 mg, 80 μ mol) and saturated NaHCO₃ (20 μ L). The reaction was monitored by TLC, which showed that starting material had disappeared after 20 min. The mixture was quenched with aqueous NaHCO₃ and extracted with dichloromethane (2 × 5 mL). The combined organic phases were washed with brine, dried over anhydrous Na₂SO₄, and purified by chromatography with EtOAc/MeOH (3:1) as eluent to give compound **11** as a colorless solid (10 mg, 47%): ¹H NMR (600 MHz, CDCl₃): $\delta = 2.28$ (s, 3H), 2.40 (m, 1H), 2.48–2.50 (m, 1H), 2.66 (m, 1H), 2.73–2.81 (m, 2H), 2.95 (m, 1H), 5.52 (m, 1H), 7.15–7.37 ppm (m, 10H); X-ray crystal structure.

4,4-Diphenyl-3-fluoro-piperidine-HCl (12): Piperidine **10** (57 mg, 0.24 mmol) dissolved in CHCl₃ (5 mL) was treated with hydrochloride gas for 2 h to form the hydrochloride salt. Recrystallization from MeOH/diethyl ether gave **12** as a white solid (58 mg, 83%): m.p. 184–185 °C; ¹H NMR (600 MHz, CDCl₃): $\delta = 2.73$ (br t, 1H), 3.07–3.12 (m, 2H), 3.50

(m, 1H), 3.57 (d, $J = 14$ Hz, 1H), 3.78 (t, $J = 11$ Hz, 1H), 6.21–6.28 (m, 1H), 7.25–7.49 ppm (m, 10H); MS (FAB⁺): m/z : 256.3; X-ray crystal structure.

N-Methyl-4,4-diphenyl-3-fluoropiperidine-TFA (13): Piperidine **11** was taken up in [D₆]DMSO and its proton and ¹³C NMR spectra recorded. Subsequently, two drops of trifluoroacetic acid (TFA) were added to the NMR tube and the corresponding spectra of the salt were recorded. See Table 3 and Table 4 for the spectra. No attempt was made to isolate the compound beyond this exercise.

N,N-Dimethyl-3-fluoro-4,4-diphenylpiperidinium iodide (14): Compound **10** (79 mg, 0.31 mmol) was treated with potassium hydroxide (119 mg, 2.12 mmol) in acetone. The reaction mixture was refluxed for 20 min, then iodomethane (1 mL) was added dropwise to the mixture. After refluxing for 2 h, the reaction mixture was filtered and the filtrate was evaporated to furnish a white solid; recrystallization from MeOH/diethyl ether delivered **14** as a white solid (90 mg, 71%): m.p. 278–280 °C; ¹H NMR (600 MHz, D₂O): $\delta = 3.04$ –3.17 (m, 2H), 3.12 (s, 3H), 3.33 (s, 3H), 3.34–3.37 (m, 2H), 3.68 (d, $J = 13$ Hz, 1H), 3.83 (dd, $J = 15, 39$ Hz, 1H), 4.08 (t, $J = 12$ Hz, 1H), 6.29 (m, 1H), 6.27–7.50 ppm (m, 10H); MS (FAB⁺): m/z : 284.4 [M–I]⁺; elemental analysis calcd (%) for C₁₉H₂₃FN: C 55.47, H 5.60, N 3.41; found: C 54.89, H 5.62, N 3.36; X-ray crystal structure.

N,N-Dimethyl-4,4-diphenylpiperidinium iodide (17): 1-Methyl-4-piperidone (**15**) (8.0 mmol, 0.9 g) was dissolved in dry benzene (5 mL), treated with TfOH (5 mL), and stirred at room temperature for 3 h. The reaction mixture was then poured into ice-water, neutralized with NaHCO₃ (s), and extracted with CHCl₃ (3 × 10 mL). The combined organic phase was washed with brine, dried with MgSO₄, and concentrated in vacuo to give diphenylpiperidine **16** (2.0 g) as a white solid (quantitative yield), which was used for the next step without further purification. Compound **17** was prepared by refluxing a solution of **16** (251 mg, 1.0 mmol) in CH₂Cl₂ (5 mL) and CH₃I (1.0 mL) for 1 h. After removal of the solvent, the residue was recrystallized from MeOH/diethyl ether to obtain a light yellow solid **17**^[37] (350 mg, 89%): m.p. 302–303 °C; MS (FAB⁺): m/z : 266.4 [M–I]⁺; X-ray crystal structure.

NMR spectroscopy: For the detailed structural work on piperidines **11**, **12**, **13**, and **14** the NMR data was collected on a Varian INOVA-400 high-resolution NMR spectrometer equipped with a 5-mm Nalorac 4N Plus probe. The ¹H, ¹³C, and ¹⁹F observation frequencies were 400, 100, and 376 MHz, respectively. Samples were dissolved in [D₆]DMSO (Isotec) and run in 5-mm NMR tubes (Wilmad 535) at 25 °C. The carbon-13 multiplicity was deduced from the gradient-enhanced-HSQC (gHSQC) heterocorrelation data, the APT (attached proton test), and/or the DEPT-135 experiments. All other two-dimensional experiments (gCOSY, gNOESY, gHMOC) were the gradient-enhanced versions^[38] as provided in the Varian VNMR 6.1B version of the software.

Crystal structure analysis: The best available crystals of **11**, **12**, **14**, and **17** were coated with Paratone N oil, suspended in small fiber loops, and placed in a cooled nitrogen gas stream at 100 K on a Bruker D8 SMART 1000 CCD sealed tube diffractometer with graphite-monochromated Cu_{K α} (1.54178 Å) radiation. Data were measured by using a series of combinations of phi and omega scans with 10 s frame exposures and 0.3° frame widths, except for **11** that had 30 s frame times. Data collection, indexing, and initial cell refinements were all carried out using SMART^[39] software. Frame integration and final cell refinements were done by using SAINT^[40] software. All four data sets were corrected for absorption using the program SADABS.^[41]

The structures were solved by using direct methods and difference Fourier techniques (SHELXTL, V5.10).^[42] The hydrogen atoms were located in difference Fourier maps or positioned by using the HFIX command in SHELXTL, and were included in the final cycles of least-squares with isotropic U_{ij} values. All non-hydrogen atoms were refined anisotropically in **11** and **17**, but in **12** and **14** only the F, Cl, N and I, F atoms, respectively, were anisotropically refined. Scattering factors and anomalous dispersion corrections are taken from the *International Tables for X-ray Crystallography*.^[43] Structure solution, refinement, graphics and generation of publication materials were performed by using SHELXTL, V5.10 software.

CCDC-247306–CCDC-247309 contain the supplementary crystallographic data for compounds **11**, **12**, **14** and **17**, respectively, in this paper. These data can be obtained free of charge via www.ccdc.cam.ac.uk/conts/retrieving.html (or from the Cambridge Crystallographic Data Centre, 12 Union Road, Cambridge CB2 1EZ, UK; fax: (+44) 1223-336-033; or e-mail: deposit@ccdc.cam.ac.uk).

Computational aspects Molecular mechanics calculations were carried out with MacroModel 6.5.^[44] Ab initio and DFT calculations were performed with the Gaussian 98 series of programs.^[45] All structures were geometry-optimized either with the solvent-enhanced MMFF/GBSA/H₂O force field (MacroModel 6.5), the DFT method Becke3LYP/6-311G(d,p) or the latter coupled to the Tomasi continuum solvation model for water^[18] (PCM), that is, Becke3LYP/6-311G(d,p)/PCM. Single-point calculations were performed at three levels of theory: Becke3LYP/6-31G*/MMFF/GBSA/H₂O, Becke3LYP/6-311G(d,p)/MMFF/GBSA/H₂O, or MP2/6-311G(d,p)/PCM//Becke3LYP/6-311G(d,p)/PCM. The HF/6-31G* electrostatic surfaces of Figure 4 and Figure 5 were generated within Spartan 02^[46] from the MMFF-optimized structures. Conformer populations were calculated by using a Boltzmann distribution at 298 K (or other temperature when specified). Unit cell analysis leading to Figure 6 and Figure 7 were performed with CCD's Mercury program.^[47]

Acknowledgements

A.S. and J.P.S. are grateful to Professor Dennis Liotta (Emory University) for generous encouragement and support. We are also appreciative to the NIH for providing support for an X-ray diffractometer (NIH S10-RR13673).

- [1] E. L. Eliel, S. H. Wilen, *Stereochemistry of Organic Compounds*, Wiley, New York, **1994**.
- [2] F.-A. Kang, C.-L. Yin, *J. Am. Chem. Soc.* **1997**, *119*, 8562–8563.
- [3] a) F. A. L. Anet, J. Krane, W. Kitching, D. Doddrell, D. Praeger, *Tetrahedron Lett.* **1974**, *15*, 3255–3258; b) P. F. Barron, D. Doddrell, W. J. Kitching, *J. Organomet. Chem.* **1977**, *6*, 361–383; c) K. Kwetkat, W. J. Kitching, *J. Chem. Soc. Chem. Commun.* **1994**, 345–347.
- [4] a) B. Cornett, M. Davis, S. Wu, N. Nevins, J. P. Snyder, *J. Am. Chem. Soc.* **1998**, *120*, 12145–12146; b) M. C. Davis, B. Cornett, S. Wu, J. P. Snyder, *J. Am. Chem. Soc.* **1999**, *121*, 11864–11870.
- [5] E. L. Eliel, S. H. Wilen, *Stereochemistry of Organic Compounds*, Wiley, New York, **1994**, pp. 686–726, 740–754.
- [6] *Conformational Behavior of Six-Membered Rings*, (Ed.: E. Juaristi), VCH Publishers, **1995**.
- [7] D. C. Lankin, N. S. Chandrakumar, S. N. Rao, D. P. Spangler, J. P. Snyder, *J. Am. Chem. Soc.* **1993**, *115*, 3356–3357.
- [8] J. P. Snyder, N. S. Chandrakumar, H. Sato, D. C. Lankin, *J. Am. Chem. Soc.* **2000**, *122*, 544–545.
- [9] D. C. Lankin, G. L. Grunewald, F. A. Romero, I. Y. Oren, J. P. Snyder, *Org. Lett.* **2002**, *4*, 3557–3560.
- [10] a) C. H. Bushweller in *Conformational Behavior of Six-Membered Rings*, (Ed.: E. Juaristi), VCH Publishers, **1995**, Ch 2, p. 25; b) E. L. Eliel, S. H. Wilen, *Stereochemistry of Organic Compounds*, Wiley, New York, **1994**, p. 696.
- [11] For example, Becke3LYP/6-311G(d,p) optimization of (CH₃)₄N⁺ leads to the following Mulliken charge distribution: N –0.32, C –0.20, H +0.18. Within the NBO framework,^[12,25] the charges for the same structure are: Becke3LYP, N –0.31, C –0.35, H +0.23; MP2, N –0.29, C –0.32, H +0.21.
- [12] E. D. Glendenning, A. E. Reed, J. E. Carpenter, F. Weinhold, NBO Version 3.1 as implemented in Gaussian 98;^[45] A. E. Reed, L. A. Curtiss, F. Weinhold, *Chem. Rev.* **1988**, *88*, 899–926; cf. <http://www.chem.wisc.edu/~nbo5/>
- [13] D. S. Balley, J. A. Walder, J. B. Lambert, *J. Am. Chem. Soc.* **1972**, *94*, 177–180.
- [14] A. Bondi, *J. Phys. Chem.* **1964**, *68*, 441–451.
- [15] The C–C bond lengths in cyclohexane by electron diffraction are 1.536 Å,^[16] while a combined ED and microwave study for piperidine found the C–N bond separations to be 1.472 Å.^[17]
- [16] O. Bastiansen, L. Fernholt, H. M. Seip, H. Kambara, K. Kuchitsu, *J. Mol. Struct.* **1973**, *18*, 163–168, and references therein.
- [17] G. Gunderson, D. W. H. Rankin, *Acta Chem. Scand. Ser. A* **1983**, *37*, 865–874.
- [18] a) S. Miertus, E. Scrocco, J. Tomasi, *Chem. Phys.* **1981**, *55*, 117–129; b) M. Cossi, V. Barone, R. Cammi, J. Tomasi, *Chem. Phys. Lett.* **1996**, *255*, 327–335; c) M. T. Cancès, V. Mennucci, J. Tomasi, *J. Chem. Phys.* **1997**, *107*, 3032–3041; d) V. Barone, M. Cossi, J. Tomasi, *J. Chem. Phys.* **1997**, *107*, 3210–3221; e) V. Barone, M. Cossi, J. Tomasi, *J. Comput. Chem.* **1998**, *19*, 404–417; as implemented in Gaussian 98.^[46]
- [19] a) T. A. Halgren, *J. Comput. Chem.* **1996**, *17*, 490–519; b) T. A. Halgren, *J. Comput. Chem.* **1996**, *17*, 616–641; c) T. A. Halgren, R. B. Nachbar, *J. Comput. Chem.* **1996**, *17*, 587–615; d) T. A. Halgren, *J. Comput. Chem.* **1999**, *20*, 730–748.
- [20] M. B. van Niel, I. Collins, M. S. Beer, H. B. Broughton, S. K. F. Cheng, S. C. Goodacre, A. Heald, K. L. Locker, A. M. MacLeod, D. Morrison, C. R. Moyes, D. O'Connor, A. Pike, M. Rowley, M. G. N. Russell, B. Sohal, J. A. Stanton, S. Thomas, H. Verrier, A. P. Watt, J. L. Castro, *J. Med. Chem.* **1999**, *42*, 2087–2104.
- [21] D. A. Klumpp, M. Garza, A. Jones, S. Mendoza, *J. Org. Chem.* **1999**, *64*, 6702–6705.
- [22] J. B. Lambert, H. F. Shurvell, D. A. Lightner, R. G. Cooks, *Organic Structural Spectroscopy*, Prentice Hall, New Jersey, **1998**, pp. 47–48.
- [23] a) H. L. Holland, *Tetrahedron Lett.* **1978**, *19*, 881–882; b) J. T. Nelson, L. J. Kurz, *Magn. Reson. Chem.* **1993**, *31*, 203–213.
- [24] J.-P. Berthelot, J.-C. Jacquesy, J. Levisalles, *Bull. Soc. Chim. Fr.* **1971**, 1896–1902.
- [25] C. Thibaudeau, J. Plavec, J. Chattopadhyaya, *J. Org. Chem.* **1998**, *63*, 4967–4984.
- [26] S. M. Bachrach in *Reviews in Computational Chemistry, Vol. 5* (Eds.: K. B. Lipkowitz, D. B. Boyd), Wiley-VCH, New York, **1994**, pp. 171–268.
- [27] The charges that correspond to the electrostatic potential surfaces (ESP) of Figure 5 and **S5** are somewhat different from Natural/NBO and Mulliken charges. Specifically, negative charge on nitrogen is redistributed to hydrogen atoms on C–H bonds, leading to a positive charge at nitrogen for **2a** and **26**. Thus, the figures illustrate a positive charge distribution (“blue”) in the vicinity nitrogen. Nonetheless, the ESP charges at F and the spatially closest methyl groups are very similar to the NBO and Mulliken charges: **2a** (C)H–F, +0.22 (H) and –0.32 (F); **26** (C)H–F, +0.09, +0.16 (H) and –0.31, –0.32 (F). Consequently, in the two figures, the green-red interface corresponds to the (N)H–F(C) interactions.
- [28] a) R. D. Stolow, T. W. Giants, J. D. Roberts, *Tetrahedron Lett.* **1968**, *9*, 5777–5780; b) R. D. Stolow, T. Groom, P. D. McMaster, *Tetrahedron Lett.* **1968**, *9*, 5781–5784.
- [29] Y. Terui, K. Tori, *J. Chem. Soc. Perkin Trans. 2* **1973**, 127–133.
- [30] R. J. Abraham, C. J. Medforth, P. E. Smith, *J. Comput.-Aided Molec. Des.* **1991**, *5*, 205–212.
- [31] a) E. L. Eliel, H. D. Banks, *J. Am. Chem. Soc.* **1972**, *94*, 171–176; b) E. L. Eliel, H. D. Banks, *J. Am. Chem. Soc.* **1972**, *94*, 8587–8589; c) E. L. Eliel, F. Alcudia, *J. Am. Chem. Soc.* **1974**, *96*, 1939–1941.
- [32] a) *Biomedical Aspects of Fluorine Chemistry*, (Eds.: R. Filler, Y. Kobayashi), Elsevier, New York, **1982**; b) *Biomedical Frontiers of Fluorine Chemistry*, (Eds.: I. Ojima, J. R. McCarthy, J. T. Welch), ACS Symposium Series No. 639, Washington D. C., **1996**; c) D. O'Hagan, H. S. Rzepa, *Chem. Commun.* **1997**, 645–652; d) B. K. Park, N. R. Kitteringham, P. M. O'Neill, *Annu. Rev. Pharmacol. Toxicol.* **2001**, *41*, 443–470.
- [33] α_2 -Adrenoreceptor ligands: a) G. L. Grunewald, V. H. Dahanukar, R. K. Jalluri, K. R. Criscione, *J. Med. Chem.* **1999**, *42*, 1982–1990; b) G. L. Grunewald, T. M. Caldwell, Q. Li, K. R. Criscione, *J. Med. Chem.* **1999**, *42*, 3588–3601; c) G. L. Grunewald, T. M. Caldwell, Q. Li, K. R. Criscione, *J. Med. Chem.* **2001**, *44*, 2849–2856;

- d) G. L. Grunewald, F. A. Romero, K. R. Criscione, *J. Med. Chem.* **2004**, ASAP, DOI: 10.1021/jm049594x.
- [34] Serotonin-subtype receptor ligands: a) See reference [20]; b) D. J. Hallett, U. Gerhard, S. C. Goodacre, L. Hitzel, T. J. Sparey, S. Thomas, M. Rowley, *J. Org. Chem.* **2000**, *65*, 4984–4993; c) M. Rowley, D. J. Hallett, S. Goodacre, C. Moyes, J. Crawforth, T. J. Sparey, S. Patel, R. Marwood, S. Patel, S. Thomas, L. Hitzel, D. O'Connor, N. Szeto, J. L. Castro, P. H. Hutson, A. M. MacLeod, *J. Med. Chem.* **2001**, *44*, 1603–1614.
- [35] a) H. S. Duewel, E. Daub, V. Robinson, J. F. Honek, *Biochemistry* **2001**, *40*, 13167–13176; b) J. Feeney, J. E. McCormick, C. J. Dauer, B. Birdsall, C. M. Moody, B. A. Starkmann, D. W. Young, P. Francis, R. H. Havlin, W. D. Arnold, E. Oldfield, *J. Am. Chem. Soc.* **1996**, *118*, 870–876.
- [36] W. Still, M. Kahn, A. Mitra, *J. Org. Chem.* **1978**, *43*, 2923–2925.
- [37] N. Sperber, M. Sherlock, D. Papa, *J. Am. Chem. Soc.* **1953**, *75*, 1122–1124.
- [38] a) T. Parella, *Magn. Reson. Chem.* **1998**, *36*, 467–495; b) W. F. Reynolds, R. G. Enriquez, *J. Nat. Prod.* **2002**, *65*, 221–244.
- [39] SMART Version 5.55, **2000**, Bruker AXS, Inc., Analytical X-ray Systems, 5465 East Cheryl Parkway, Madison WI 53711–5373.
- [40] SAINT Version 6.02, **1999**, Bruker AXS, Inc., Analytical X-ray Systems, 5465 East Cheryl Parkway, Madison WI 53711–5373.
- [41] SADABS, **1996**, George Sheldrick, University of Göttingen.
- [42] SHELXTL V5.10, **1997**, Bruker AXS, Inc., Analytical X-ray Systems, 5465 East Cheryl Parkway, Madison WI 53711–5373.
- [43] *International Tables for X-ray Crystallography, Volume C*. (Ed.: A. J. C. Wilson), Kynoch, Academic Publishers, Dordrecht, **1992**, Tables 6.1.1.4 (pp. 500–502) and 4.2.6.8 (pp. 219–222).
- [44] F. Mohamadi, N. G. J. Richards, W. C. Guida, R. Liscamp, M. Lipton, C. Caufield, G. Chang, T. J. Hendrickson, W. C. Still, *J. Comput. Chem.* **1991**, *12*, 1110–1117; cf. <http://www.schrodinger.com/Products/macromodel.html>
- [45] M. J. Frisch, et al.; Gaussian 98 (Revision A.1), Gaussian, Inc, Pittsburgh PA, 1998; cf. <http://www.gaussian.com/>
- [46] Spartan '02, Wavefunction, Inc.; Irvine, CA; cf. <http://www.wavefunction.com>
- [47] Mercury software; CSD version 5.24 (November 2002); cf. <http://www.ccdc.cam.ac.uk>

Received: August 13, 2004
Published online: January 20, 2005